Summary of the 2020 Asian Summer Monsoon

1. Precipitation and temperature

CLIMAT data on four-month total precipitation for the summer monsoon season (June – September) show more than 140% of the normal in the eastern part of East Asia, the southeastern part of Southeast Asia and southern/western parts of South Asia, while values less than 60% of the normal were seen in the northeastern part of Southeast Asia and western China (Figure 3-1 (a)). Seasonal precipitation in China from June to August was the second highest since 1961 (China Meteorological Administration), and monthly precipitation in western/eastern Japan for July was the highest since 1946. Heavy rain caused more than 270 fatalities or people missing in China from June to August (Chinese Government), 84 fatalities in Japan in July (Fire and Disaster Management Agency of Japan) and more than 2,200 fatalities in/around South Asia from June to September (governments of India/Nepal/Pakistan, European Commission).

Four-month mean temperatures for the same period were above normal in many parts of Asia, while values were below normal in and around the northwestern part of East Asia (Figure 3-1 (b)). Monthly mean temperatures in western and eastern Japan for August were the highest since 1946. Heat waves caused a total of 112 fatalities in Japan from June to September (Fire and Disaster Management Agency of Japan).

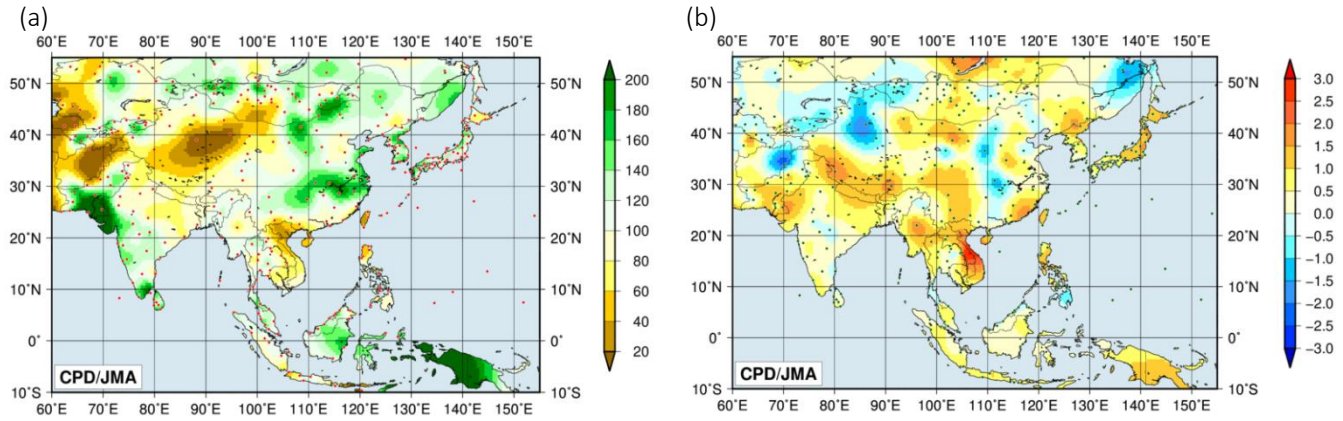

Figure 3-1 Four-month (a) precipitation ratios [%] and (b) mean temperature anomalies [°C] from June to September 2020
The base period for the normal is 1981 – 2010. The red (a) and green (b) dots show stations providing map data, which are interpolated due to a lack of CLIMAT reporting and climatological normal values in some areas.

2. Tropical cyclones

A total of 13 named tropical cyclones (TCs) had formed over the western North Pacific and the South China Sea by September 2020, as compared to the normal of 18.4 (Table 3-1). From June to September, 12 named TCs (climatological normal: 16.0) formed, with 10 approaching or making landfall on East Asia and 6 (climatological normal: 9.2) approaching Japan. No named TCs formed in July for the first time since 1951.

Between late August and early September, 3 TCs (Bavi, Maysak and Haishen) reaching TY intensity passed by Okinawa/Amami and made landfall on the Korean Peninsula.

Table 3-1 Tropical cyclones reaching TS intensity or higher formed over the western North Pacific and the South China Sea by September 2020

Name (number)		Date (UTC)	Category[1)]	Maximum wind[2)] (kt)
Vongfong	(2001)	12 May - 16 May	TY	85
Nuri	(2002)	12 Jun - 13 Jun	TS	40
Sinlaku	(2003)	1 Aug - 2 Aug	TS	40
Hagupit [3)]	(2004)	1 Aug - 5 Aug	TY	70
Jangmi [3)]	(2005)	8 Aug - 10 Aug	TS	45
Mekkhala [3)]	(2006)	10 Aug - 11 Aug	STS	50
Higos [3)]	(2007)	18 Aug - 19 Aug	STS	55
Bavi [3)]	(2008)	22 Aug - 27 Aug	TY	85
Maysak [3)]	(2009)	28 Aug - 3 Sep	TY	95
Haishen [3)]	(2010)	1 Sep - 7 Sep	TY	100
Noul [3)]	(2011)	15 Sep - 18 Sep	TS	45
Dolphin [3)]	(2012)	21 Sep - 24 Sep	STS	60
Kujira [3)]	(2013)	27 Sep - 30 Sep	STS	60

Note: Based on information from the RSMC Tokyo-Typhoon Center.
1) Intensity classification for tropical cyclones.
TS: tropical storm, STS: severe tropical storm, TY: typhoon
2) Estimated maximum 10-minute mean wind.
3) Based on early analysis data, but not best track.

3. Monsoon activity and atmospheric circulation

Convective activity inferred from OLR averaged for June – September 2020 (Figure 3-2) was enhanced over the western tropical Indian Ocean and the Maritime Continent, and was suppressed from the northern part of Southeast Asia to the central equatorial Pacific in association with higher-than-normal SSTs in the tropical Indian Ocean and La Niña conditions in the equatorial Pacific (Figure 3-3). OLR index data (Table 3-2) indicate that the overall activity of the Asian summer monsoon (represented by the SAMOI (A) index) was below normal, and the active convection area was shifted southward (SAMOI (N) index) and westward (SAMOI (W) index) of its normal position except in August.

In the upper troposphere (Figure 3-4 (a)), cyclonic circulation anomalies straddling the equator were seen over the Maritime Continent, while anti-cyclonic circulation anomalies straddling the equator were seen from Africa to the central Indian Ocean with the westward extension of the Tibetan High. The southward displacement of the subtropical jet stream (STJ) over Eurasia was related to weaker-than-normal northward extension of the Tibetan High, which is likely attributable to the suppressed convective activity observed over the monsoon region. A wave train along the STJ was seen, with cyclonic circulation anomalies over Central Asia and anti-cyclonic circulation anomalies over southern China and to the east of Japan.

In the lower troposphere (Figure 3-4 (b)), cyclonic circulation anomalies straddling the equator were seen over the western tropical Indian Ocean, while anti-cyclonic circulation anomalies straddling the equator were seen from the eastern tropical Indian Ocean to the western tropical Pacific. The North Pacific Subtropical High (NPSH) extended southwestward of its climatological extent, and the monsoon trough over Southeast Asia was weaker than normal. Figure 3-5 shows northeasterly surface wind anomalies extending from the northeastern Indian Ocean to the western

tropical North Pacific, which imply low-level divergence anomalies over areas from the South China Sea to the western tropical North Pacific. The lower-tropospheric divergence anomalies gave rise to descending air flow and suppressed convective activity over these areas, which likely contributed to the southwestward extension of the NPSH.

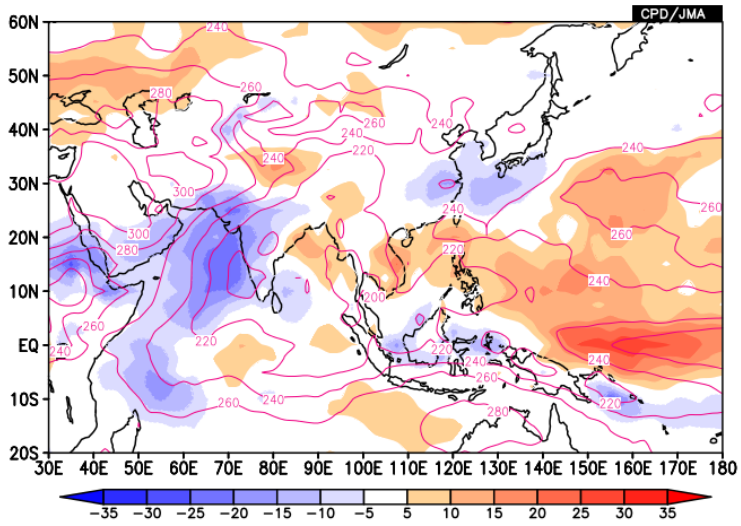

Figure 3-2 Four-month mean outgoing longwave radiation (OLR) [W/m^2] for June–September 2020
The contours indicate OLR at intervals of 20 W/m^2, and the color shading denotes OLR anomalies from the normal (i.e., the 1981–2010 average). Negative (cold color) and positive (warm color) OLR anomalies show enhanced and suppressed convection compared to the normal, respectively. Original data are provided by NOAA.

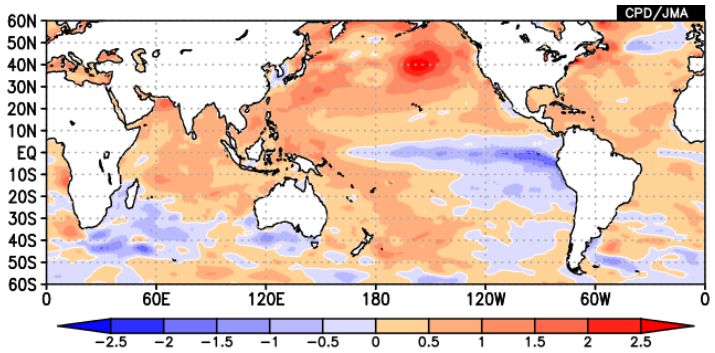

Figure 3-3 Four-month mean sea surface temperature (SST) anomalies [°C] for June–September 2020
The base period for the normal is 1981 – 2010.

Table 3-2 Summer Asian Monsoon OLR Index (SAMOI) values observed from May to September 2020
Asian summer monsoon OLR indices (SAMOI) are derived from OLR anomalies. SAMOI (A), (N) and (W) indicate the overall activity of the Asian summer monsoon, its northward shift and its westward shift, respectively. SAMOI definitions are as follows: SAMOI (A) = (-1) × (W + E); SAMOI (N) = S – N; SAMOI (W) = E – W. W, E, N and S indicate area-averaged OLR anomalies for the respective regions shown in the figure on the right normalized by their standard deviations.

	Summer Asian Monsoon OLR Index (SAMOI)		
	SAMOI (A): Activity	SAMOI (N): Northward-shift	SAMOI (W): Westward-shift
May 2020	-1.0	-1.4	+0.8
Jun 2020	-0.7	-1.0	+0.3
Jul 2020	-1.7	-0.8	+0.2
Aug 2020	-0.9	+1.7	-0.2
Sep 2020	-0.1	-0.3	+1.9

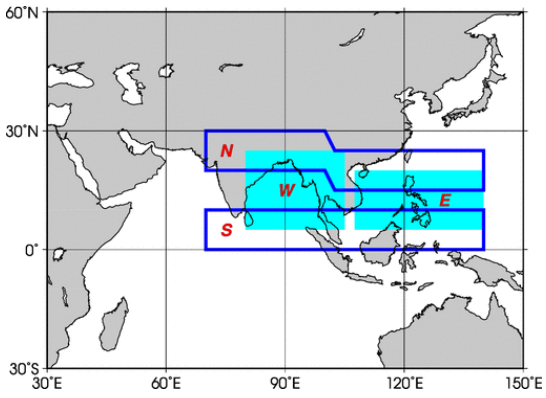

(a) (b)

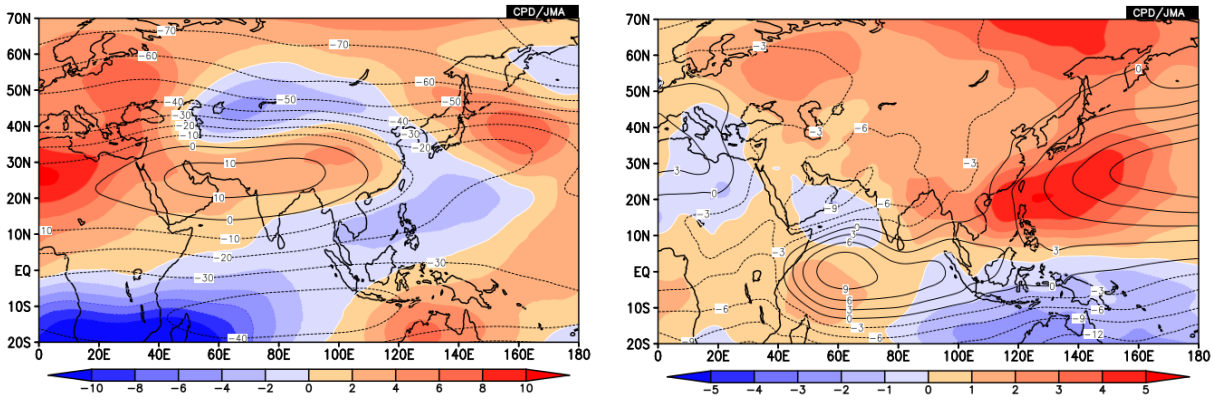

Figure 3-4 Four-month mean (a) 200-hPa and (b) 850-hPa stream function [10^6 m^2/s] for June–September 2020
Contours indicate stream function at intervals of (a) 10 × 10^6 m^2/s and (b) 3 × 10^6 m^2/s, and shading shows stream function anomalies. Red (blue) shading denotes anti-cyclonic (cyclonic) circulation anomalies in the Northern Hemisphere, and vice-versa in the Southern Hemisphere. The base period for the normal is 1981 – 2010.

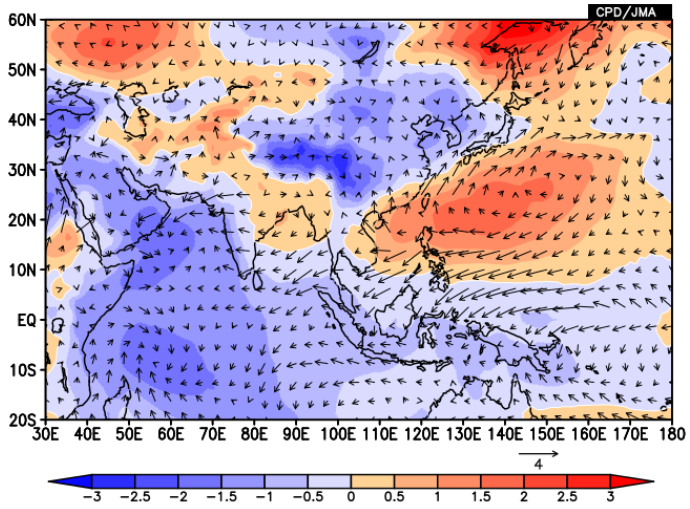

Figure 3-5 Sea level pressure anomalies (color shading) [hPa] and surface wind vector anomalies (vectors) [m/s] for June–September 2020.
The base period for the normal is 1981 – 2010.

In July 2020, areas from western to northeastern Japan experienced record-heavy rain and record-low sunshine durations. These phenomena are attributed to a continued tendency for large amounts of water vapor to concentrate around western and eastern Japan from two major flows (Figure 3-6) – one from the west along the active Meiyu-Baiu front, which stagnated from central China to mainland Japan due to delayed northward migration of the STJ, and the other from the southwest along the periphery of the NPSH, which extended southwestward of its climatological extent (Figure 3-7). A persistent upper-level trough over the Yellow Sea, which was sustained by quasi-stationary Rossby wave propagation along the STJ over Eurasia (Figure 3-7 (a)), also caused an intensification of Meiyu-Baiu front activity with enhanced vertical upward flow over western and eastern Japan, resulting in prolonged heavy rain.

In August 2020, the STJ migrated northward over East Asia due to the northward shift of active convection over the Asian monsoon region, and also meandered northward over Japan due to Rossby wave propagation along the STJ with a geographical phase different from that observed in July. In association with this meandering, the NPSH and the Tibetan High expanded toward Japan and brought record-high temperatures in western and eastern parts of the country via strengthened downward flow and predominant sunny conditions.

(a) (b)

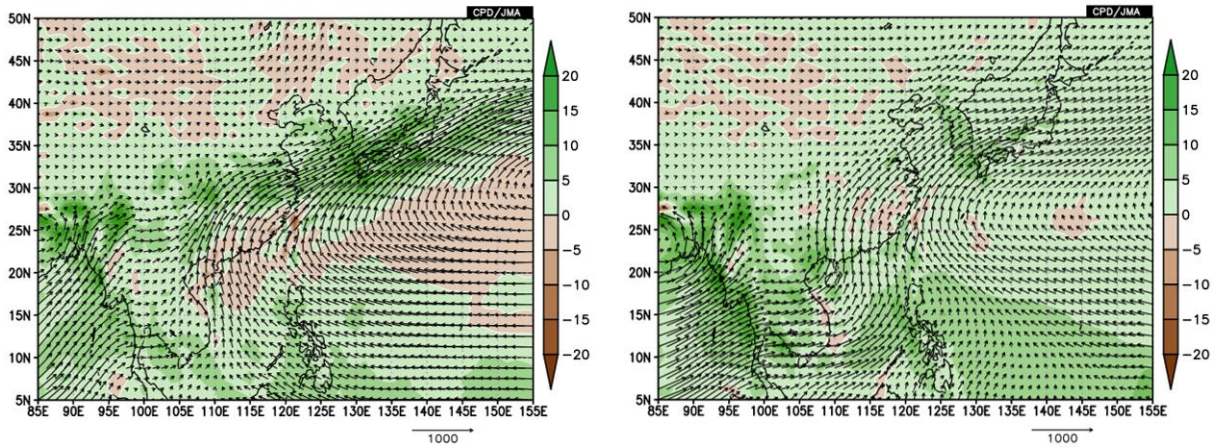

Figure 3-6 Monthly mean vertically integrated horizontal water vapor flux (arrows) and related convergence (color shading): (a) July 2020; (b) normal

Unit: kg/m/s for arrows and mm/day for shading. Green (brown) shading denotes convergence (divergence). Vertical integration is up to 300 hPa. The base period for the normal is 1981 – 2010.

(a) (b)

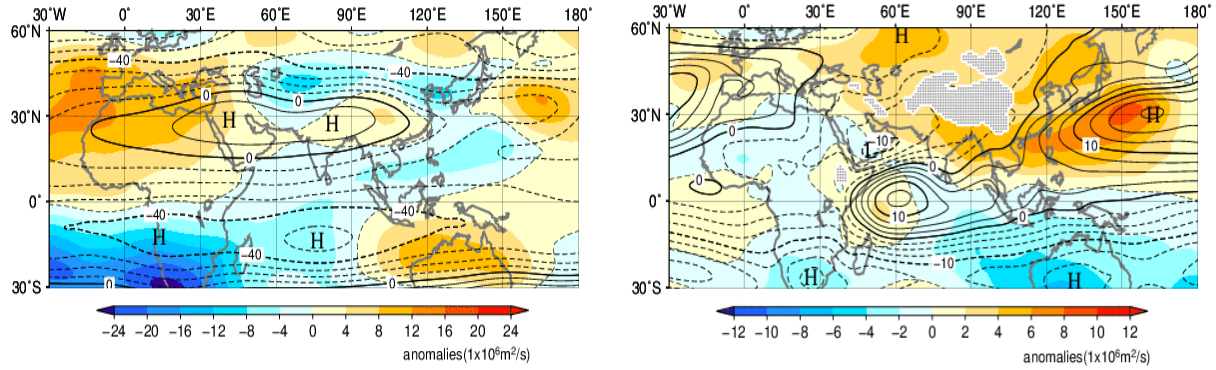

Figure 3-7 Monthly mean (a) 200-hPa and (b) 850-hPa stream function [10^6 m^2/s] for July 2020

Contours indicate stream function at intervals of (a) 10×10^6 m^2/s and (b) 2.5×10^6 m^2/s, and shading shows stream function anomalies. Hatch patterns indicate areas with altitudes exceeding 1,600 m. The base period for the normal is 1981 – 2010.

(SATO Hitoshi, Tokyo Climate Center)

<<Table of contents <Top of this article